The differential-algebraic Windkessel model with power as input

Pigot, Harry; Soltesz, Kristian

Published in:
2022 American Control Conference (ACC)

DOI:
10.23919/ACC53348.2022.9867889

2022

Document Version:
Peer reviewed version (aka post-print)

The differential-algebraic Windkessel model with power as input

Henry Pigot[1] and Kristian Soltesz[1]

Abstract— **The lack of methods to evaluate mechanical function of donated hearts in the context of transplantation imposes large precautionary margins, translating into a low utilization rate of donor organs. This has spawned research into cyber-physical models constituting artificial afterloads (arterial trees), that can serve to evaluate the contractile capacity of the donor heart. The Windkessel model is an established linear time-invariant afterload model, that researchers committed to creating a cyber-physical afterload have used as a template. With aortic volumetric flow as input and aortic pressure as output, it is not directly obvious how a Windkessel model will respond to changes in heart contractility. We transform the classic Windkessel model to relate power, rather than flow, to pressure. This alters the model into a differential-algebraic equation, albeit one that is straightforward to simulate. We then propose a power signal model, that is based on pressure and flow measurements and optimal in a Bayesian sense within the class of C2 signals. Finally, we show how the proposed signal model can be used to create relevant simulation scenarios, and use this to illustrate why it is problematic to use the Windkessel model as a basis for designing a clinically relevant artificial afterload.**

I. Introduction

Heart evaluation in isolation from the body can help ensure that donor organs are safe prior to initiating transplantation, lowering costs and patient risk. At present, one heart preservation and evaluation system is clinically available, wherein the heart beats empty (unloaded) providing only metabolic indicators of heart function [1]. Such indicators have shown poor correlation to post-transplant outcomes compared to functional metrics[2], [3]. Functional evaluation of donor hearts enables direct observation of hemodynamic performance, giving clinicians insight into how well an organ will perform in a recipient.

Recent advances by our collaborators in nonischemic organ preservation extend the admissable *ex vivo* (out-of-body) time for heart organs from 4 h to 24 h [4], [5]. This extended admissible time opens up for the use of extended-criteria donors [6], [7], and enables functional donor heart evaluation within the time constraints of the transplantation procedure.

Functional evaluation requires a supply of perfusate to the heart ventricles, as well as an artificial cardiac afterload for the heart to beat against. The afterload must maintain diastolic aortic pressure to ensure coronary flow and limit systolic pressure to a safe limit, while subjecting the heart to physiological loading conditions. Afterloads are commonly built as verbatim implementations of the common arterial Windkessel model, combining discrete resistive and compliant elements as an approximation of the arterial tree [8]. Some groups have implemented adjustable elements enabling computer control of mean aortic pressure, as in [9], or manual adjustment of systolic and diastolic pressure, as in [10].

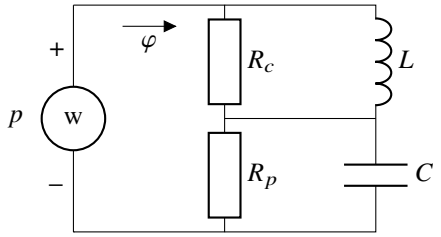

Fig. 1. Circuit diagram equivalent of the 4-element parallel Windkessel model with parameters $\theta = [R_p\ C\ R_c\ L]^\top$, aortic flow (current) φ, and pressure (voltage) p. The heart is modeled as a power source w, as opposed to the flow (current) source utilized in the classic Windkessel formulation.

In simulation of cardiac afterloads, changes in contractility (defining the forcefullness of heart beats) and arrhythmic conditions (irregular heart beats) are of foremost interest for evaluating heart function under a given loading condition. Here we investigate how an artificial afterload model, implemented as a Windkessel model, can be expected to behave when subjected to contractile changes and arrhythmia.

Julia code that can reproduce all results herein is available on GitHub [11].

II. Differential-algebraic Windkessel model

A. Flow input Windkessel

The classic "lumped-parameter" Windkessel impedance is a low-order (at most two) LTI model that estimates aortic pressure $p(t)$ by $\hat{p}(t)$ based on aortic volumetric flow $\varphi(t)$ [8]. Here we will consider the most general of these, the 4-element parallel Windkessel model [12]. The circuit diagram of its electric analogy, with electric current representing volumetric flow and electric potential (voltage) representing pressure, is shown in Fig. 1. A state space realization of the

*This work was partially funded by the Swedish Research Council (grant 2017-04989) and the Swedish Foundation for Strategic Research (grant SM21-0037). The authors are members of the ELLIIT Strategic Research Area at Lund University.

[1]Department of Automatic Control, Lund University, P.O. Box 118, SE 221-00, Lund, Sweden henry.pigot@control.lth.se, kristian.soltesz@control.lth.se

TABLE I
PARAMETERS OF THE WINDKESSEL MODEL OF FIG. 1 FROM [12].

Parameter	Value	Unit	Name
R_p	13.2	mmHg/(L/min)	Peripheral resistance
C	0.0732	L/mmHg	Compliance
R_c	0.933	mmHg/(L/min)	Characteristic resistance
L	0.085	mmHg · min/(L/min)	Inertance

system is provided by

$$\dot{x} = \underbrace{\begin{bmatrix} -\frac{1}{CR_p} & 0 \\ 0 & -\frac{R_c}{L} \end{bmatrix}}_{A} x + \underbrace{\begin{bmatrix} 1 \\ R_c \end{bmatrix}}_{B} \varphi, \tag{1a}$$

$$p = \underbrace{\begin{bmatrix} \frac{1}{C} & -\frac{R_c}{L} \end{bmatrix}}_{C} x + \underbrace{\begin{bmatrix} R_c \end{bmatrix}}_{D} \varphi. \tag{1b}$$

(Context will decide when C refers to the compliance parameter or state space output matrix.) In the physiology literature, the parameters

$$\theta = [R_p \ C \ R_c \ L]^\top > 0 \tag{2}$$

are ascribed mechanistic properties as per Tab. I.

The parameters are typically identified from aortic volumetric flow samples $\varphi_1, \ldots, \varphi_n$ and corresponding aortic pressure samples $p_1, \ldots, p_n$ simultaneously sampled at $t_1 < \cdots < t_n$. The sampling instances are chosen so that consecutive samples are sufficiently close in time to resolve the dynamics to be modeled, and $t_n - t_1$ typically spans either an integer number of cardiac cycles, or one cardiac cycle that is periodically extended as in [13]. Identification of θ is most commonly cast as an output-error minimization, with quadratic cost on $p_k - \hat{p}(t_k)$, see *e.g.* [14].

B. Power input Windkessel

The Windkessel model provides a dynamic relation between aortic volumetric flow and aortic pressure, that matches observations well [14]. It is therefore not surprising that research prototypes of artificial dynamic afterloads (adjustable arterial tree models) to be used in functional *ex vivo* evaluation of donor hearts [9], [10], [15]–[17], have been constructed to emulate the dynamics of the Windkessel model.

While the Windkessel model employs a volumetric flow source model of the heart, a power source model is much more relevant to our investigations of contractile function variations and arrhythmia. The work exerted by the left ventricle on the blood being ejected in one cardiac cycle is the area of a Carnot cycle, referred to in the literature as a pressure-volume loop, or just a PV-loop. The work w associated with transitioning from ventricular volume v_1 to v_2 along this cycle is

$$w(v_1, 2_2) = -\int_{v_1}^{v_2} p(v) \ dv. \tag{3}$$

To be accurate, (3) provides an upper bound for this work, and that bound is tight for lossless systems. Letting t_1 and t_2 be the times corresponding to v_1 and v_2, such that $v(t_1) = v_1$), the work of (3) can be expressed as

$$w(t_1, t_2) = -\int_{t_1}^{t_2} p(t)\frac{dv}{dt}dt = -\int_{t_1}^{t_2} \varphi(t)p(t) \ dt. \tag{4}$$

In the PV-loop context, flow into the left ventricle (from the left atrium) is considered. Here, we are instead considering flow out of the left ventricle (through the aorta). We therefore employ (4) with a sign change of its right-hand-side, and conclude that the instantaneous power is

$$w = \varphi p. \tag{5}$$

Assuming for now that $\hat{p} = p$, i.e., that the Windkessel model captures the afterload dynamics perfectly, we can use (1b) together with (5) to algebraically relate the instantaneous power w to the flow φ through

$$w = (Cx + D\varphi)\varphi = Cx\varphi + D\varphi^2. \tag{6}$$

Combining (6) with (1) results in the nonlinear differential-algebraic equation (DAE)

$$\dot{x} = Ax + B\varphi \tag{7a}$$

$$w = Cx\varphi + D\varphi^2. \tag{7b}$$

The DAE (7) has index one (since there is no differentiation of its input, w), and is therefore readily solvable by numerical DAE integrators. The algebraic equation (7b) has solutions

$$\varphi = \frac{-Cx \pm \sqrt{(Cx)^2 + 4Dw}}{2D}, \tag{8}$$

meaning that any initial condition $x(t_0)$ fulfilling $(Cx(t_0))^2 + 4Dw(t_0) \geq 0$ is feasible (while others are not). In particular $x(t_0) = 0$ is feasible.

III. POWER SIGNAL MODEL

In this section we formulate a statistical signal estimation problem that is solved by employing cubic spline smoothing. To be notationally coherent and reproducible, we have chosen to explicitly include a small review of related topics.

A. Smoothing cubic splines

We consider modeling of the heart power input signal w from sampled flow φ and pressure p time series. The zero-order-hold (ZOH) interpolation is the default choice when sampled signals are considered in the context of control systems. Indeed it makes sense if the signal source is a digital controller, that maintains steady output levels between invocations. However, physiological signals seldom exhibit ZOH behavior. Instead, they are (with some exceptions such as neuronal signalling) smooth. We therefore assume that our samples are observations of some unknown C^2 (twice

differentiable, with continuous second derivative) signal, that we aim to estimate.

Based on observations $y = [y_1 \ \dots \ y_n]^\top$ of an unknown signal $x(t)$, sampled at times $\tau = [t_1 \ \dots, t_n]^\top$, we hence want to obtain a C^2 signal model $\hat{x}$ of x on (t_1, t_n) with $\chi = [\hat{x}(t_1) \ \dots \ \hat{x}(t_n)]^\top$.Since we have no information about x between samples, we choose as objective to minimize the roughness

$$\rho(\hat{x}(t)) = \int_\tau \ddot{\hat{x}}(t) \ dt. \tag{9}$$

One can note that this is similar, but generally not identical to, minimizing total curvature, that is defined as the integral of $\ddot{\hat{x}}$ along the curve, integrating dl rather than dt.

If our observations have not been corrupted by noise, we are searching for the least rough C^2 curve x that passes through the *knots* defined by τ and $\chi = y$. That curve is the natural cubic spline generated by (τ, χ) [18]. It is a piecewise cubic polynomial $\hat{x}(t) = \hat{x}_k(t)$, where

$$\begin{aligned} &\hat{x}_k(t) = \alpha_k + \beta_k(t - t_k) + \gamma_k(t - t_k)^2 + \delta_k(t - t_k)^3, \\ &t_k \le t < t_{k+1}, \ k = 1, \dots, n-1, \end{aligned} \tag{10}$$

uniquely defined by the parameter $\theta = [\alpha^\top \ \beta^\top \ \gamma^\top \ \delta^\top]^\top$, with column vectors on the form $\alpha = [\alpha_1 \ \dots \ \alpha_{n-1}]^\top$. Particularly, the spline polynomials defined through (10) are linear in θ.

The spline is defined to pass through the knots, where its first and second derivatives are continuous. This corresponds to the constraints

$$\hat{x}_k(t_{k+1}) = \hat{x}_{k+1}(t_k) = \chi_k, \tag{11a}$$

$$\dot{\hat{x}}_k(t_{k+1}) = \dot{\hat{x}}_{k+1}(t_k), \tag{11b}$$

$$\ddot{\hat{x}}_k(t_{k+1}) = \ddot{\hat{x}}_{k+1}(t_k), \tag{11c}$$

holding for $k = 1, \dots, n-1$. The constraints (11) uniquely define the always existing cubic spline down to boundary conditions. The two types of boundary conditions we will consider are *natural* (a.k.a. normal or ordinary) and *periodic*. The natural spline has zero second derivatives at its end-points

$$\ddot{\hat{x}}(t_1) = \ddot{\hat{x}}(t_n) = 0. \tag{12}$$

It is called natural because originally, when flexible rulers constrained by nails at the knot, were used to draw splines, leaving the ruler unconstrained beyond the end-points would correspond to the condition (12).

Many physiological signals, including cardiac cycles, are periodic to their nature, and it can therefore be desirable to extrapolate periodically using data covering (at least) one period.

The natural spline is not necessarily C^2 across the period boundary. However, replacing (12) with explicit C^2 constraints on the end-points

$$\hat{x}(t_1) = \hat{x}(t_n), \tag{13a}$$

$$\dot{\hat{x}}(t_1) = \dot{\hat{x}}(t_n), \tag{13b}$$

$$\ddot{\hat{x}}(t_1) = \ddot{\hat{x}}(t_n), \tag{13c}$$

equivalently results in an existing and uniquely defined spline.

It is reasonable to assume that our measurements y of x are corrupted by noise ϵ, so that $y = x + \epsilon$. In our formulation we will use the relevant case where ϵ is a realization of a zero-mean processes with covariance Σ. We note that it is sufficient to consider predictive performance at the instances defined by τ, since the cubic spline (normal or periodic) is uniquely defined by the knot abscissas χ at these ordinates. We could choose χ so the knots end up on a straight line. This results in a cubic spline of zero roughness. However, since $\mathbb{E}\epsilon = 0$, any choice but $\chi = y$ is associated with an estimation bias. In estimating x_k, this bias is simply $y_k - \chi_k$. On the other end of the scale we have $\chi = y$, which provides an unbiased estimator at the cost of higher variance.

As we will shortly see χ is linear in θ and minimizing the smoothing cubic spline cost

$$J(\theta; \lambda) = \lambda \underbrace{(y - \chi(\theta))^\top \hat{\Sigma}^{-1} (y - \chi(\theta))}_{J_1} + (1 - \lambda) \underbrace{\rho(\chi(\theta))}_{J_2} \tag{14}$$

balances between reducing bias (second term) and variance (first term) through the parameter $\lambda \in (0, 1)$. If $\epsilon \sim \mathcal{N}(0, \Sigma)$ and $\hat{\Sigma} = \Sigma$, the minimizer χ of J_1 is the maximum likelihood estimator (MLE) of y. By parametrizing J as convex combination of J_1 and J_2, we are left with determining λ within the closed interval $(0, 1)$, as opposed to the interval $(0, \infty)$ associated with the common formulation $J = J_1 + \lambda J_2$ (where λ is now another parameter with the same role).

Returning to the spline fitting problem, the C^2 conditions can be encoded into a linear equation system

$$S\gamma = 3V\alpha \tag{15}$$

in the knot values $\alpha_k = \chi_k$ and knot second derivatives $\ddot{\chi}_k = 2\gamma_k$, each defined for $k = 1, \dots, n-1$ [18]. The matrices S and V are constructed from t. Introducing $h_k = x_{k+1} - x_k$ and $q_k = 1/h_k$ where $k = 1, \dots, n-1$, the matrices corresponding to the periodic case are

$$S = \begin{bmatrix} 2\Delta h_{n-1} & h_1 & & & & & & \\ h_1 & 2\Delta h_1 & h_2 & & & & & \\ \vdots & \vdots & \vdots & \vdots & \vdots & \vdots & \vdots & \\ & & & & h_{n-3} & 2\Delta h_{n-3} & h_{n-2} & \\ h_{n-1} & & & & & h_{n-2} & 2\Delta h_{n-2} & \end{bmatrix}, \tag{16a}$$

$$V = \begin{bmatrix} -\Delta q_{n-1} & q_1 & & & & & & q_{n-1} \\ q_1 & -\Delta q_1 & q_2 & & & & & \\ \vdots & \vdots & \vdots & \vdots & \vdots & \vdots & \vdots & \\ & & & & q_{n-3} & -\Delta q_{n-3} & q_{n-2} & \\ q_{n-1} & & & & & q_{n-2} & -\Delta q_{n-2} & \end{bmatrix}, \tag{16b}$$

where $\Delta(\cdot)_k = (\cdot)_k + (\cdot)_j$ with $j = (\max((k+1)\%n), 1)$.

The natural counterparts are obtained by setting

$$S_{1,n-1} = S_{n-1,1} = S_{1,2} = S_{n-1,n-2} = 0, \tag{17a}$$

$$V_{1,n-1} = V_{n-1,1} = V_{1,1} = V_{1,2} = 0, \tag{17b}$$

in (16a) and (16b), respectively. Using that $\alpha_k = \chi_k$ we can express the first term of (14) as

$$J_1 = (y - \alpha)^\top \hat{\Sigma}^{-1} (y - \alpha), \tag{18}$$

and as mentioned in *e.g.* [18], the roughness of the cubic spline on (t_1, t_n) can be expressed

$$J_2 = \frac{2}{3}\gamma^\top S\gamma. \tag{19}$$

The objective (14) is therefore a quadratic form in α:

$$J = \lambda(y-\alpha)^\top(y-\alpha) + (1-\lambda)6\alpha^\top V^\top S^{-\top} V\alpha, \tag{20}$$

that can be written on the standard form

$$J = \frac{1}{2}a^\top U\alpha - v^\top\alpha + r, \tag{21}$$

with

$$U = 2\lambda\hat{\Sigma}^{-1} + 12(1-\lambda)V^\top S^{-\top}V, \tag{22a}$$
$$v = 2\lambda\hat{\Sigma}^{-1}y, \tag{22b}$$
$$r = \lambda y^\top\hat{\Sigma}^{-1}y. \tag{22c}$$

Minimizing (21) with respect to α (i.e. also with respect to θ) is an ordinary least squares problem, and the unique minimizer is the solution to $U\alpha = v$. Having obtained α, it is then possible to obtain the remaining parameters from the end-point constraints through the following equations that (after some manipulation) follow from the definition of the smoothing cubic spline:

$$\gamma = 3S^{-1}V\alpha, \tag{23a}$$
$$\delta = \frac{1}{3}H^{-1}D\gamma, \tag{23b}$$
$$\beta = H^{-1}D\alpha - H\gamma - H^2\delta, \tag{23c}$$

where $H = \operatorname{diag}(h)$ and

$$D = \begin{bmatrix} -1 & 1 & & & & \\ & -1 & 1 & & & \\ \vdots & \vdots & \vdots & \vdots & \vdots & \vdots \\ 1 & & & & & -1 \end{bmatrix} \tag{24}$$

B. Choice of smoothing parameter

The remaining question is how to choose the smoothing parameter $\lambda \in (0,1)$, that constitutes a bias–variance trade-off. Using all available data for training, there is no way to determine whether one candidate is favorable to another (except for subjectively by looking at the resulting fit). A frequently used way to determine λ is therefor through leave-one-out cross validation. The predictive performance is measured as the mean square error over $k = 1, \ldots, n$ in predicting y_k with a predictor that has been trained on all data except (t_k, y_k):

$$J_\lambda = \frac{1}{n}\sum_{k=1}^{n}\left(y_k - \hat{x}^{(-k)}(t_k)\right)^2. \tag{25}$$

Here, $\hat{x}^{(-k)}$ denotes a cubic spline fitted to all data but (t_k, y_k), and since the spline is a function of the smoothing parameter λ, we can minimize J_λ over λ. A celebrated result [19] enables cheap evaluation through

$$J_\lambda = \sum_{k=1}^{n-1}\left(\frac{y_k - \hat{x}(t_k)}{1 - W_{kk}}\right)^2, \tag{26}$$

where $\chi = Wy$ defines the smoothing matrix

$$W = \begin{bmatrix} w_1^\top \\ \vdots \\ w_n^\top \end{bmatrix} = \begin{bmatrix} 2\lambda U^{-1} \\ w_n^\top \end{bmatrix}. \tag{27}$$

The last row $w_n^\top$ of the right-hand-side of (27) corresponds to y_n. For the periodic case we therefore have $w_n = w_1$. For the natural case, w_n is instead obtained through (23). Alternatively, one could introduce γ_n as an explicit variable in the natural counterpart to (16), in which case the right-hand-side would be simply $2\lambda U^{-1}$.

It is also worth noting that the effective degree of freedom resulting from the regularization is $\operatorname{Tr} W$, making it monotonic in λ. That does not imply that J_λ lacks local minima, but for practical purposes it often suffices to determine λ through bisection search over $(0, 1)$, which is what we do in the upcoming examples.

C. Modeling heart power

We realistically assume that our φ and p measurement time series are time-aligned and corrupted by additive independent Gaussian noise drawn from $\mathcal{N}(0, \sigma_\varphi^2)$ and $\mathcal{N}(0, \sigma_p^2)$, respectively. Even if the time series are synchronized (which they do not need to be), we fit individual smoothing cubic splines $\hat{\varphi}$ and $\hat{p}$, and use $\hat{w} = \hat{\varphi}\hat{p}$ to model w in (7), to preserve the MLE property of the fitted curves.

For any time t where both splines $\hat{\varphi}$ and $\hat{p}$ are defined, their product $\hat{w}$ is the product of two third-order polynomials that we can explicitly compute. As a direct consequence, $\hat{w}$ will also be C^2 and we can compute $\dot{\hat{w}}(t)$ and $\ddot{\hat{w}}(t)$ analytically from the underlying splines. Particularly, if $\hat{\varphi}$ and $\hat{p}$ have a coinciding end-point with a natural end-point condition, then $\hat{w}$ will have have a coinciding end-point with natural end-point condition.

It also follows directly from the definition that if $\hat{\varphi}$ is periodic with T_φ and $\hat{p}$ is periodic with T_p, then $\hat{w}$ will be periodic unless T_φ/T_p is irrational, with period at least $\max(T_\varphi, T_p)$ and at most $\operatorname{lcm}(T_\varphi, T_p)$. If $T = T_\varphi = T_p$, then $\hat{w}$ will be periodic with period (evenly dividing) T. The noise variance σ^2 just shifts the balance between J_1 and J_2 in (14), in a way that can be compensated for using λ. We therefore fix $\sigma_p^2 = \sigma_\varphi^2 = \sigma^2 = 1$ and leave it up to the cross validation to suggest a λ that minimizes its approximation of the expected prediction error.

IV. Simulation examples

Implementing the DAE (7) within the `Julia DifferentialEquations.jl` suite and providing its right-hand-side with $w = \hat{w}$, modeled as described in Sec. III, we simulate the Windkessel with power input

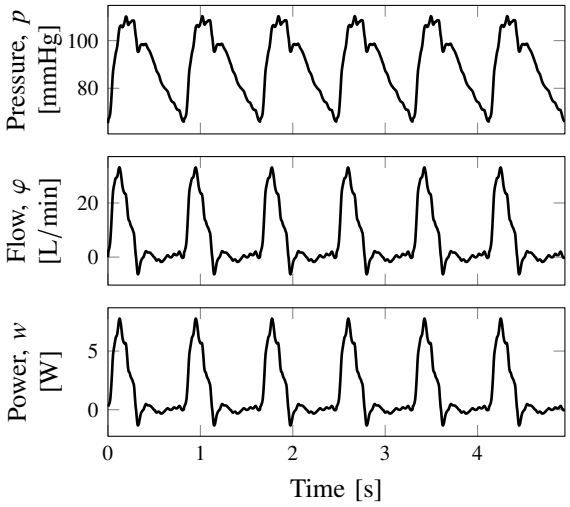

Fig. 2. Windkessel DAE simulation with periodically extended power input w. Top panes show the resulting pressure p and flow φ.

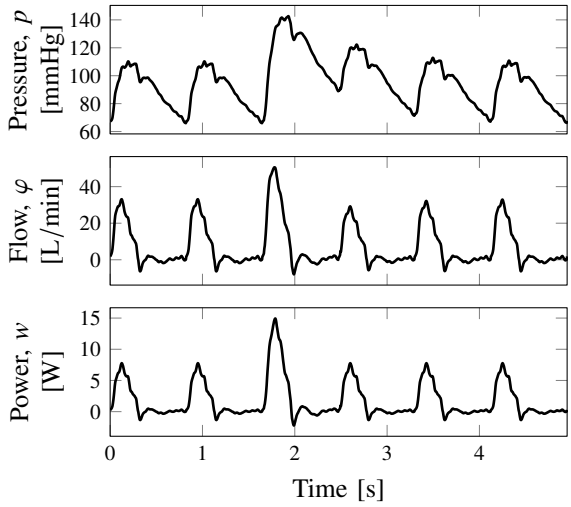

Fig. 3. Windkessel DAE simulation with double contractile strength (power w) in beat 3. Top panes show the resulting pressure p and flow φ.

using the `Sundials.jl` DAE integrator. Our simulations are based on digitized waveforms from [12], representing homeostatic human aortic volumetric flow and aortic pressure, respectively, as further explained in [13].

A. Periodic input

As a first example, we simulate a train of cardiac cycles, by evaluating the periodic extension of the φ and p splines, and forming $w = \varphi p$ pointwise from these. Fig. 2 shows w, and the resulting φ and p from simulating with the DAE Windkessel model. The initial state of the DAE has been selected for transient elimination by solving a two-point boundary value problem, enforcing the DAE states at the beginning and end of one cardiac cycle to match. Another possibility is to set $x(0) = 0$ (or other feasible value), simulate sufficiently long for any transient to fade, and then truncate. The system matrix A of (1) has eigenvalues $-1/(CR_p)$ and $-Rc/L$ corresponding to poles with time constants $T_1 = CR_p$ =1 min and L/R_c =5.5 s. If the cardiac cycle duration is T_c, each state component has therefore reached within $100e^{-t}$ % of its "transient free" value within $l\lceil t/T_c \rceil$ cardiac cycles.

1) Varying contractility: Fig. 3 illustrates the flow and pressure response to a beat with increased contractile strength. The input was generated by adding an offset spline to the w spline of Fig. 2 to double the amplitude of the 3rd beat.

2) Arrhythmic event: Fig. 4 illustrates the response to an arrhythmic event. The input was generated by shifting the w spline abscissas of Fig. 2 back 0.7 cycle periods after beat 3. (This does not exactly correspond to a physiologically correct PVC, but serves to illustrate that we can alter a nominal power input by arbitrary offsets in magnitude and time.)

V. Discussion

We have proposed expressing the Windkessel model as a DAE, to use instantaneous power, rather than volumetric flow, as its input. This has enabled us to investigate how the dynamics react to changes in contractility and arrhythmia.

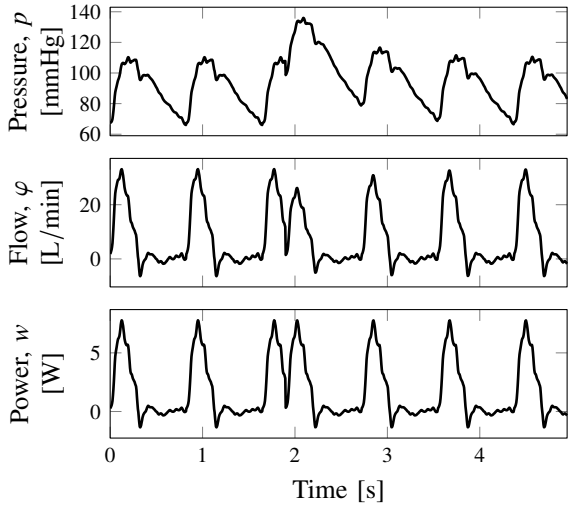

Fig. 4. Windkessel DAE simulation with an early contraction in beat 4 of the input power w. Top panes show the resulting pressure p and flow φ.

To handle flow and pressure measurements only being available at time-aligned, but not necessarily synchronized nor evenly spaced sampling instances, a continuous time signal model was employed. This signal model constitutes the MLE estimator under the assumption that the underlying singnals are C^2 and corrupted with additive identically independently distributed Gaussian noise. Regularization was added to avoid possible overfitting, and its extent determined through cross validation.

Our simulation examples show how the considered Windkessel model responds to changes in heart contractility and double-beat arrhythmia. These events notably affect the resulting pressure profile. As a consequence of the Windkessel dynamics, there is no simple relation between the model parameters (2) and the resulting diastolic and systolic pressure.

Compensating through feedback control of the Windkessel model parameters to maintain prescribed safe upper systolic pressure and lower diastolic pressure bounds as proposed in [10] is therefore non-trivial, and motivates investigation of artificial afterloads based on other principles than a verbatim implementation of Windkessel dynamics.

VI. Conclusion

- Its volumetric flow input makes the classic lumped-parameter Windkessel model ill-suited for investigating how changes in contractility affect aortic pressure. For this purpose, a DAE representation with instantaneous power as input is more adequate.
- Smoothing cubic splines constitute a motivated class of functions for modeling aortic flow and pressure signal from sampled data. These models can readily be combined into a power signal model that maintains the smoothness properties of the cubic spline.
- It is desirable, but not straightforward, to independently control diastolic and systolic pressure within a Windkessel model with adjustable parameters.

References

[1] A. Ardehali, F. Esmailian, *et al.*, "Ex-vivo perfusion of donor hearts for human heart transplantation (PROCEED II): A prospective, open-label, multicentre, randomised non-inferiority trial," *The Lancet*, vol. 385, no. 9987, pp. 2577–2584, 2015.

[2] C. W. White, E. Ambrose, *et al.*, "Assessment of donor heart viability during ex vivo heart perfusion," *Canadian Journal of Physiology and Pharmacology*, vol. 93, no. 10, pp. 893–901, 2015.

[3] R. V. P. Ribeiro, J. S. Alvarez, *et al.*, "Comparing Donor Heart Assessment Strategies During Ex Situ Heart Perfusion to Better Estimate Posttransplant Cardiac Function," *Transplantation*, vol. 104, no. 9, pp. 1890–1898, 2020.

[4] S. Steen, A. Paskevicius, *et al.*, "Safe orthotopic transplantation of hearts harvested 24 hours after brain death and preserved for 24 hours," *Scandinavian Cardiovascular Journal*, vol. 50, no. 3, pp. 193–200, 2016.

[5] G. Qin, B. Wohlfart, *et al.*, "Intact coronary and myocardial functions after 24 hours of non-ischemic heart preservation," *Scandinavian Cardiovascular Journal*, vol. 54, no. 1, pp. 59–65, 2020.

[6] K. Soltesz, T. Sjöberg, *et al.*, "Closed-loop regulation of arterial pressure after acute brain death," *Journal of Clinical Monitoring and Computing*, vol. 32, no. 3, pp. 429–437, 2018.

[7] Y. Wahlquist, K. Soltesz, *et al.*, "Prevention of Ischemic Myocardial Contracture Through Hemodynamically Controlled DCD," *Cardiovascular Engineering and Technology*, 2021.

[8] N. Westerhof, J.-W. Lankhaar, *et al.*, "The arterial Windkessel," *Medical & Biological Engineering & Computing*, vol. 47, no. 2, pp. 131–141, 2009.

[9] A. Fisher, R. E. Challis, *et al.*, "A controllable artificial afterload for isolated heart studies," *Journal of Biomedical Engineering*, vol. 6, no. 4, pp. 305–310, 1984.

[10] B. Gellner, L. Xin, *et al.*, "The Implementation of an Adjustable Afterload Module for Ex Situ Heart Perfusion," *Cardiovascular Engineering and Technology*, vol. 11, no. 1, pp. 96–110, 2020.

[11] H. Pigot, *Power-windkessel*, commit 8dac16a, 2022. [Online]. Available: `https://github.com/hpigot/power-windkessel/tree/v1.0.0` (visited on 03/14/2022).

[12] N. Stergiopulos, B. E. Westerhof, *et al.*, "Total arterial inertance as the fourth element of the windkessel model," *American Journal of Physiology-Heart and Circulatory Physiology*, vol. 276, no. 1, H81–H88, 1999.

[13] H. Pigot, J. Hansson, *et al.*, "Identification of cardiac afterload dynamics from data," in *11th IFAC Symposium on Biological and Medical Systems BMS 2021*, accepted (forthcoming): IFAC-PapersOnLine, 2021.

[14] P. Segers, E. Rietzschel, *et al.*, "Three-and-four-element Windkessel models: Assessment of their fitting performance in a large cohort of healthy middle-aged individuals," *Proceedings of the Institution of Mechanical Engineers. Part H, Journal of engineering in medicine*, vol. 222, pp. 417–28, 2008.

[15] E. Seifen, A. B. Seifen, *et al.*, "Comparison of cardiac effects of enflurane, isoflurane, and halothane in the dog heart-lung preparation," *Journal of Cardiothoracic Anesthesia*, vol. 1, no. 6, pp. 543–553, 1987.

[16] J.-M. Abicht, T. Mayr, *et al.*, "Large-Animal Biventricular Working Heart Perfusion System with Low Priming Volume—Comparison between in vivo and ex vivo Cardiac Function," *The Thoracic and Cardiovascular Surgeon*, vol. 66, no. 01, pp. 071–082, 2018.

[17] J. de Hart, A. de Weger, *et al.*, "An ex vivo platform to simulate cardiac physiology: A new dimension for therapy development and assessment," *The International Journal of Artificial Organs*, vol. 34, no. 6, pp. 495–505, 2011.

[18] C. De Boor, "A Practical Guide to Splines (Revised Edition)," in, Springer, 2001, pp. 207–214, ISBN: 978-0-387-90356-9.

[19] B. W. Silverman, "A Fast and Efficient Cross-Validation Method for Smoothing Parameter Choice in Spline Regression," *Journal of the American Statistical Association*, vol. 79, no. 387, pp. 584–589, 1984.

Acknowledgment

This work was funded by the Swedish Research Council (grant 2017-04989) and the Swedish Foundation for Strategic Research (grant SM21-0037). We would like to acknowledge our collaborators with the Division of Thoracic Surgery at Lund University, and Jonas Hansson with the Department of Automatic Control, who inspired us to use smoothing splines for signal modeling.